Cellular Signalling 20 (2008) 1769–1779

Contents lists available at ScienceDirect

Cellular Signalling

journal homepage: www.elsevier.com/locate/cellsig

Identification of a novel di-leucine motif mediating K^+/Cl^- cotransporter KCC2 constitutive endocytosis

Beibei Zhao [a], Adrian Y.C. Wong [b], Ayesha Murshid [a], Derek Bowie [b], John F. Presley [a], Fiona Kay Bedford [a,*]

[a] Department of Anatomy & Cell Biology, McGill University, Montreal, Quebec, Canada
[b] Pharmacology & Therapeutics, McGill University, Montreal, Quebec, Canada

ARTICLE INFO

Article history:
Received 3 March 2008
Received in revised form 10 June 2008
Accepted 12 June 2008
Available online 24 June 2008

Keywords:
KCC2
Chloride transporter
Endocytosis
AP-2

ABSTRACT

The neuron-specific potassium-chloride cotransporter 2 (KCC2) plays a crucial role, by controlling chloride extrusion, in the development and maintenance of inhibitory neurotransmission. Although it is now well established that activity-dependent mechanisms can down regulate KCC2 gene expression, the role of post-translational mechanisms in controlling KCC2 expression, specifically at the cell-surface, are poorly understood. We therefore set out to identify the mechanisms and motifs regulating KCC2 endocytosis, one important pathway that may control KCC2 membrane expression. Using a fluorescence-based assay, we show KCC2 when expressed in HEK293 cells is constitutively internalized via a dynamin- and clathrin-dependent pathway. Consistent with this, we demonstrate KCC2 from adult mouse brain associates in vivo with the clathrin-binding adaptor protein-2 (AP-2) complex. Using an endocytosis reporter system, we identify the presence of an autonomous endocytosis motif in the carboxyl cytoplasmic terminus of KCC2. By site-directed mutagenesis we define this novel KCC2 endocytic motif as a non-canonical di-leucine motif, $_{657}$LLXXEE$_{662}$. Finally by mutating this motif in the context of full-length KCC2 we demonstrate that this novel KCC2 endocytic motif is essential for the constitutive internalization of KCC2 and for binding to the AP-2 complex. Subsequent sequence analysis reveals this motif is highly conserved between the closely related K^+/Cl^- family members that mediate chloride efflux, but absent from the more distant related cotransporters controlling chloride influx. In conclusion, our results indicate constitutive internalization of KCC2 is clathrin-mediated and dependent on the binding of AP-2 to this novel endocytic motif. Furthermore, that this process appears to be an evolutionarily conserved mechanism amongst functionally homologous cotransporters.

1. Introduction

Fast inhibitory neurotransmission is mediated by two classes of ligand gated Cl^- channels, the γ-amino-butyric acid type-A receptor ($GABA_AR$) and the glycine receptor (GlyR) [1,2]. In each case Cl^- influx is triggered upon channel opening resulting in hyperpolarization of the postsynaptic membrane. This in turn, leads to a reduction in the likelihood of further neurotransmitter release [1,2]. In the majority of neurons, Cl^- influx and fast hyperpolarizing inhibition are critically dependent on low intracellular chloride concentrations ($[Cl^-]_i$). The neuron-specific K^+–Cl^- cotransporter, KCC2, has now been identified as an essential protein in establishing and maintaining this low $[Cl^-]_i$, by controlling Cl^- extrusion [3].

During central nervous system (CNS) development, KCC2 gene expression is upregulated and underlies the transition of GABA and glycine responses from the immature depolarizing to the hyperpolarizing responses found in adults [3]. This transition occurs as the overall developmental increase in KCC2 activity leads to a reduction in $[Cl^-]_i$, which at resting membrane potentials promotes Cl^- influx (hyperpolarization) rather than efflux upon ion channel opening [3]. Further, in mature neurons a reduction in KCC2 gene expression, via antisense oligonucleotide suppression, leads to an increase in $[Cl^-]_i$ and a shift in $GABA_AR$ responses to immature depolarizing [3]. These observations have demonstrated that dynamic regulation of KCC2 gene expression can alter the direction of $GABA_AR$ and GlyR signaling. Consistent with this and its essential role in inhibition, KCC2 knockout mice die shortly after birth [4]. In addition, a loss of KCC2 expression is recognized as a contributing factor in the pathological conditions of chronic pain [5], nerve injury [6] and epilepsy [7,8].

Besides the above-mentioned regulation of KCC2 gene expression, short-term modulation of the KCC2 protein has also been demonstrated. Several kinase activities can modulate KCC2 Cl^- transport activity in both immature [9–12] and mature [13] hippocampal neurons. The precise molecular mechanisms involved however, have yet to be eluded. In addition a rapid loss of KCC2 cell surface expression has been demonstrated under conditions of increased

* Corresponding author. Department of Anatomy & Cell Biology, McGill University, 3640 University Street, Montreal, Quebec, Canada H3A 2B2. Tel.: +1 514 398 1426; fax: +1 514 398 5047.
E-mail address: fiona.bedford@mcgill.ca (F.K. Bedford).

0898-6568/$ – see front matter © 2008 Elsevier Inc. All rights reserved.
doi:10.1016/j.cellsig.2008.06.011

interictal activity [14] and oxidative stress [15]. Indicating that regulation of KCC2 membrane trafficking may be a crucial mechanism by which KCC2 function can be controlled.

KCC2 is a 12 transmembrane protein with both amino and carboxyl intracellular termini and belongs to the cation-chloride cotransporter (CCC) superfamily, which consists of one Na^+–Cl^- cotransporter (NCC), two Na^+–K^+–Cl^- cotransporters (NKCCs), and four K^+–Cl^- cotransporters (KCCs). Different CCCs exert opposite Cl^- transport activities, with NCC and NKCCs taking up Cl^-, while KCCs extrude Cl^- [16]. The functional unit of CCCs is most likely to be a dimer, as homo- and hetero-dimerization have now been demonstrated for NKCC [17], NCC [18] and KCC family proteins [19]. The molecular mechanisms regulating the membrane trafficking of any CCC family member however are presently unknown, albeit they play essential roles in controlling chloride homeostasis in multiple tissues.

The cellular mechanisms controlling the cell-surface expression of many transporters and their membrane internalization, in particular, have been shown to have a profound and dynamic effect on overall transporter activity [20,21]. As one requirement for protein internalization is an interaction with the cellular endocytic machinery, the identification of the molecular motifs governing these interactions has in several cases revealed pivotal regulatory domains within these proteins [22–24]. How KCC2 membrane expression is controlled, specifically the cellular mechanism and the molecular motifs contributing to its membrane internalization are presently unknown. Therefore in the present study we set out to investigate the mechanisms controlling the membrane internalization of KCC2. Here we report our findings, using an array of endocytosis reporter systems and site-directed mutagenesis, of the cellular mechanisms and the molecular motif within KCC2 directing its constitutive internalization from the plasma membrane.

2. Materials and methods

2.1. Antibodies

The following antibodies were used, mouse monoclonal anti-HA (HA.11, Covance, Berkeley, CA, USA), rabbit polyclonal anti-KCC2 (Upstate, Lake Placid, NY, USA), mouse monoclonal anti-IL2 receptor alpha (Tac; kindly provided by Julie Donaldson, NIH, Bethesda, MD, USA), mouse monoclonal anti-alpha adaptin-clone 8 for immunoblotting (BD Biosciences, Mississauga, ON Canada) and anti-alpha adaptin-clone AP.6 for immunoprecipitation (Affinity BioReagents, Golden CO USA). Donkey anti-mouse and anti-rabbit antibodies conjugated to Alexa-488 and Alexa-546 were from Invitrogen (Carlsbad, CA, USA), while those conjugated to peroxide from Jackson Labs (Bar Harbor, Maine, USA).

2.2. Plasmids and constructs

The full length murine KCC2 cDNA was cloned by reverse transcriptase-polymerase chain reaction (RT-PCR) from RNA of mouse forebrain, using the specific pimers forward 5′-ATAGGATCCGCCACCATGCTCAACAACCTGACGGAC-3′) and reverse (5′-TATTCTAGATCAGGAGTAGATGGTGATGACC-3′). A triple tandem copy of the influenza virus haemagglutin (HA) peptide (YPYDVPDYA) was inserted into the unique NotI restriction site in the second predicted extracellular loop of KCC2, as described for the NHE-3 transporter [25], to generate HA-KCC2. The LL657,658AA mutation was introduced by site-directed mutagenesis, using the Quick-exchange mutagenesis kit (Stratagene, La Jolla, CA, USA). The Tac backbone construct was kindly provided by Julie Donaldson (NIH). To generate the Tac chimeric deletion and mutated constructs we amplified parts of the carboxyl cytoplasmic tails of KCC2 by PCR, using the forward primer (5′- ATATCTAGACGGGGGGC GGAG-3′) and the reverse primers (see Table S1 in supplementary material). These were then cloned in-frame into an XbaI site inserted at the 3′ end of the Tac cDNA. Tac-C(LL657,658AA) and Tac-C(Y555A) were generated by site-directed mutagenesis from Tac-C. HA-tagged transferin receptor (HA-TfR, Belouzard et al., 2006) was kindly provided by Yves Rouille (Institut Pasteur de Lille, Lille Cedex, France) and the HA-TfR-KCC2 amino cytoplasmic tail chimaera generated by overlapping PCR ligation so that KCC2 (amino acids 2–102) was fused to HA-TfR (amino acids 60–760). All sequences were confirmed by the McGill and Genome Quebec innovation center. The green fluorescent (GFP) dominant negative (DN) dynamin-2 K44A construct is from Marc McNiven (Mayo Clinic College of Medicine, Rochester, MA, USA), the GFP-DN-EPS15 (lacking amino acids 95–295) and the GFP-Rab11 construct were provided by Robert Lodge (NIH, Bethesda, MD, USA), the GFP-DN-Caveolin was provided by Matthew Mulvey (University of Utah, Salt Lake City, UT, USA) and the GlyR-α1 construct is from R. Harvey (School of Pharmacy, London UK).

2.3. Cell culture and transfections

Human Embryonic Kidney 293 cells (HEK293) were maintained at 37 °C in DMEM (Invitrogen), 5% CO_2 supplemented with 10% FBS, 100 U/ml penicillin/ streptomycin and 2 mM L-glutamine. Prior to transfection, cells were plated onto poly-L-lysine coated plates or glass coverslips. Transfections were carried out with Lipofectamine 2000™ (Invitrogen). Cells were assayed 18–20 h after transfection. For electrophysiological experiments, cells were transiently transfected with either wild-type or HA-tagged KCC2, GlyR-α1 and pEGFP-N (Clontech, Mountain View, Ca, USA) at a ratio of 10:3:1, using the calcium phosphate method [26]. After 8–10 h, the cells were washed twice with phosphate buffer saline^{++} (PBS^{++} contains 1 mM $CaCl_2$ and 1 mM $MgCl_2$) and maintained in fresh medium. Electrophysiological recordings were performed 24–48 h later.

2.4. Immunoprecipitation

Whole mouse forebrain lysates were prepared from adult mice (50% C57bl6/50% ICR). Animals were rapidly decapitated and the brain homogenized in immunoprecipitation (IP) buffer (10 mM HEPES pH7.4, 25 mM NaCl, 1% Triton-X-100, 1 mM Na_3VO_4, 50 mM NaF, 1 mM PMSF, 1 μg/ml leupeptin, and 1 μg/ml pepstatin) using a glass-Teflon homogenizer for 20 strokes. Homogenates were cleared by centrifugation at 14,000 g 30 min at 4 °C. Protein concentration was determined by BCA assay (Biorad, Hercules, CA, USA). 2 mg of lysate was used for each immunoprecipitation. Antigen–antibody complexes were immunoprecipitated with 2 μg anti-KCC2, anti-α-adaptin, or pre-immune rabbit or mouse IgG bound to Protein A- or G-Sepharose (Amersham, UK) at 4 °C for 2 h, washed three times in IP buffer and eluted in Laemmli buffer at 95 °C for 5 min. Proteins were separated on 8% SDS-PAGE gels, followed by Western blotting as described previously [27] with antibodies to KCC2 and α-adaptin.

For the IPs performed from HEK293 cells, 3×10^6 cells were used for each condition. 18–20 h after transfection cells were placed on ice, washed with chilled PBS, and lysed in IP buffer (10 mM HEPES pH7.4, 25 mM NaCl, 1% Triton-X-100, 1 mM PMSF, 1 μg/ml leupeptin, and 1 μg/ml pepstatin). Solubilized cell lysates were cleared by centrifugation at 14,000 g 15 min at 4 °C. Antigen–antibody complexes were immunoprecipitated with 2 μg anti-HA or pre-immune mouse control IgG bound to Protein G-Sepharose (Amersham, UK) at 4 °C for 2 h, washed three times in IP buffer and eluted in Laemmli buffer at 95 °C for 5 min. Proteins were separated on 8% SDS-PAGE gels, followed by Western blotting as described previously [27] with antibodies to HA and α-adaptin.

2.5. Fluorescence-based endocytosis assay

Transiently transfected cells were incubated in conditioned medium containing anti-HA or anti-Tac for 30 min on ice. Cells were washed extensively and incubated at 37 °C for 15 or 30 min, fixed in 4% paraformaldehyde and then incubated in blocking buffer (PBS, 10% horse serum, and 0.5% bovine serum albumin-BSA) with Alexa 546-conjugated anti-mouse secondary antibody (Invitrogen), to label cell surface anti-Tac- or anti-HA-bound proteins. Cells were subsequently permeabilized in blocking buffer plus 0.1% Triton-X-100 and incubated with Alexa 488-conjugated anti-mouse secondary antibody (Invitrogen) to label internalized anti-Tac or anti-HA-bound proteins. After a final wash, cells were mounted on glass slides with GelTol Aqueous Mounting Medium (Thermo Scientific, Waltham, MA, USA). For cells in which a GFP-tagged protein was cotransfected following endocytosis any membrane bound antibodies were removed by incubation with citrate stripping buffer (50 mM Sodium Citrate pH 4.6, 280 mM Sucrose, 0.01 mM Deferoxamine Mesylate). Cells were then fixed, permeabilized and labeled with Alexa 546-conjugated anti-mouse secondary antibodies as described above. Confocal images were collected with a 63× objective on a Zeiss LSM 510 microscope. Endocytosis was quantified as the proportion of cells demonstrating more than 10 internal labeled puncta from 30 cells on a per experiment basis ($n=3$).

2.6. Biotinylation endocytosis assay

Transiently transfected cells pre-incubated 1 h with leupeptin (100 μg/ml) were placed on ice, washed twice with PBS^{++}, incubated 20 min with 1 mg/ml Sulfo-NHS-SS-biotin-PBS^{++}, washed three times with PBS^{++} containing 0.1% BSA, then twice with PBS^{++} alone and incubated at 37 °C for either 30 or 60 min in the continuous presence of 100 μg/ml leupeptin, unless otherwise indicated. Subsequently, cells were placed on ice washed twice with PBS^{++} and the remaining cell-surface bound biotin stripped by two washes in stripping buffer (50 mM glutathione in 75 mM NaCl, 10 mM EDTA, 1% BSA, and 0.075 M NaOH). Cells were then washed two times in PBS^{++} and lysed in lysis buffer (20 mM Tris–HCl pH7.6, 50 mM NaCl, 1 mM EDTA, 1% Triton-X-100, 0.1% SDS, 1 mM Na_3VO_4, 50 mM NaF, and 10 mM $Na_4P_2O_7$ 1 mM PMSF, 1 μg/ml leupeptin, and 1 μg/ml pepstatin) for 1 h at 4 °C. Nuclei and insoluble material were removed by centrifugation at 14,000 g, 15 min, 4 °C. Biotinylated proteins were purified on NeutrAvidin-coated beads (Pierce) at 4 °C for 2 h, washed three times with lysis buffer and eluted in Laemmli buffer at 95 °C 5 min. Proteins were separated on 8% SDS-PAGE gels, followed by Western blotting with the KCC2 antibody. Intensities of immunoreactive bands were quantified by densitometry analysis of exposed films using a Biorad GS-800 densitometer. Background intensity readings were subjected from all readings and results were expressed as a percentage of the total surface labeling for each clone.

2.7. Electrophysiological recordings

Whole-cell Gramicidin-perforated patch recordings were performed on transfected cells using thin-walled borosilicate glass pipettes (4–6 MΩ) coated with dental wax.

Cells were voltage-clamped at −60 mV and recordings started 10 min after obtaining stable electrical access to the cell. All recordings were performed using an Axopatch 200B amplifier (Axon Instruments Inc., Foster City, CA, USA), and series resistances (30–40 MΩ) were compensated by 75–80% in all experiments. Current records were filtered at 10 kHz and digitized at 50–100 kHz. The reference electrode was connected to the bath via an agar bridge of 3 M KCl. Data acquisition was performed using pClamp9 software (Axon Instruments Inc., Foster City, CA, USA), and illustrated using Origin 7 (OriginLab Corp., Northampton, MA, USA). All experiments were performed at room temperature.

External solutions contained (mM): 150 NaCl, 5 HEPES, 2 $CaCl_2$, 1 $MgCl_2$, 2% phenol red, with the osmotic pressure adjusted to 290 mOsm using sucrose. Stock solutions of Gramicidin were prepared in DMSO (50 mg/ml) and diluted into the internal solution to obtain a final concentration of 5 mg/ml just before the start of the experiment. The internal solution contained (mM): 115 NaCl, 10 NaF, 5 HEPES, 5 Na_4BAPTA, 0.5 $CaCl_2$, 1 $MgCl_2$, 10 Na_2ATP. pH was adjusted to 7.3 with 5 N NaOH, and the osmotic pressure adjusted to match the external solution. Internal solution was kept on ice throughout the experiment.

3. Results

3.1. Endogenous neuronal KCC2 interacts with the clathrin-mediated endocytic machinery

Clathrin-mediated endocytosis (CME) is a prominent mechanism by which plasma membrane proteins are internalized. It involves the recruitment of membrane proteins (cargo) by the adaptor protein-2 (AP-2), to clathrin-coated pits, which are subsequently pinched from the plasma membrane to form internalized endocytic vesicles [28]. To examine whether neuronal KCC2 interacts with the CME machinery, we tested whether the AP-2 complex is bound endogenously to neuronal KCC2 by co-immunoprecipitation. For this we prepared whole cell lysates from adult mouse brain, immunoprecipitated (IP) KCC2 with a rabbit polyclonal antibody to KCC2 and used pre-immune rabbit IgG for control immunoprecipitates (Fig. 1A, top). In a reciprocal immunoprecipitation we used a mouse monoclonal antibody to the α-adaptin subunit of the AP-2 complex and pre-immune mouse IgG was used as the control (Fig. 1A, bottom). All immunoprecipitates were then analyzed by Western blot (IB) with antibodies to KCC2 and α-adaptin. We found α-adaptin was present in the immunoprecipitates isolated with the anti-KCC2 antibody, but not in the control pre-immune IgG immunoprecipitates (Fig. 1A). Also that KCC2 was present in the immunoprecipitates isolated with the anti-α-adaptin antibody, but not the control mouse IgG. This demonstrates endogenous neuronal KCC2 is present in a complex with the CME machinery and suggests KCC2 membrane internalization may be controlled by the CME-pathway.

3.2. Generation and functional characterization of a HA-tagged version of KCC2

To begin to identify the molecular mechanisms controlling KCC2 endocytosis, we needed to establish an assay in which we could test the CME dependence of KCC2 endocytosis and map the motif(s) within KCC2 controlling its endocytosis. For this, we generated an exofacial hemagglutinin (HA)-tagged KCC2, in which a triple HA tag was inserted into the second predicted extracellular loop of KCC2 (Fig. 1B). This construct would enable us to visually detect the endocytosis of KCC2 using a fluorescence-based antibody uptake assay (see below). As the CME cellular machinery including AP-2 is conserved between different cell types, we chose to use human embryonic kidney 293 (HEK293) cells for our analysis. The advantage of using this cellular system compared to neurons, which endogenously express KCC2, is their ease of manipulation. Furthermore HEK293 cells are used routinely to map CME dependent endocytosis motifs in a wide range of neuronal proteins [23,29,30].

First of all, we ensured that insertion of the triple HA epitope tag in the second extracellular loop of KCC2 did not affect the maturation or cell surface expression of KCC2 (data not shown). To also make certain the HA tag did not disrupt transporter activity we examined the

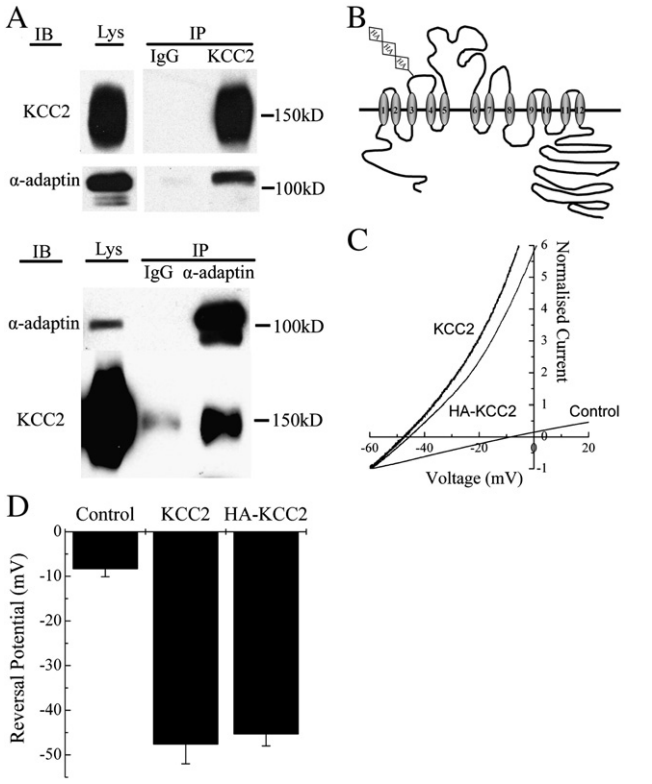

Fig. 1. Endogenous neuronal KCC2 and the clathrin adaptor protein-2 (AP-2) complex interact. (A) Mouse whole brain lysate (Lys) was immunoprecipitated (IP) with antibodies to KCC2 and control pre-immune rabbit IgG (top) or the AP-2 complex α-adaptin subunit and control mouse IgG (bottom), and Western blotted (IB) with antibodies to KCC2 or α-adaptin (B) Schematic of HA epitope-tagged KCC2. Three tandem copies of an influenza virus HA peptide (YPYDVPDYA) were inserted into the second extracellular loop of mouse KCC2. (C) Functional characterization of HA epitope-tagged KCC2. Current–voltage (IV) plots in the absence (control) and presence of either KCC2 or HA-KCC2. Note the negative shift in E_{gly} observed when either KCC2 or the HA-KCC2 construct are co-expressed with human α1 glycine receptor subunits. (D) Summary bar graph showing the effect of both KCC2 and HA-KCC2 on E_{gly}. Data are mean ± s.e., of at least 3 experiments in all conditions.

transport activity of HA-KCC2 in HEK293 cells. Using the Gramidicin perforated-patch recording technique to avoid artefactual changes in intracellular chloride concentration [31], we measured the reversal potential (E_{gly}) of homomeric human α1 glycine receptors as a means to estimate $[Cl^-]_i$ and thus KCC2 transport activity. Voltage ramps from −60 to +60 mV (500 ms duration) were given before and during bath application of 1 mM Glycine and subtracted off-line to measure E_{Gly}. In perforated-patch recordings from HEK293 cells ($n \geq 3$), co-expression of KCC2 resulted in a negative shift of E_{gly} from −8.3 ± 1.8 mV to −47 ± 4.4 mV (Fig. 1C,D), in agreement with a previous report [9]. A similar shift of E_{gly} to −45 ± 2.7 mV was also observed when HA-KCC2 was expressed (Fig. 1C,D), confirming that the HA tag does not affect the ability of KCC2 to transport Cl^- ions. Therefore, the HA-tagged version of the KCC2 construct was used as a substitute for wild-type KCC2 for all subsequent studies.

3.3. HA-KCC2 is internalized by clathrin-mediated endocytosis in HEK293 cells

To follow HA-KCC2 endocytosis in HEK293 cells we used a fluorescence-based endocytosis protocol, as outlined in Fig. 2A, in which HA-KCC2 internalization is visualized via HA.11 monoclonal antibody uptake. After 15 min of anti-HA uptake rapid constitutive internalization of HA-KCC2 was visualized (Fig. 2B, middle panel), with anti-HA labeling localized predominantly to discrete puncta underlying the plasma membrane. After 30 min however the majority

of the internal anti-HA labeling now localized to a compact perinuclear compartment (Fig. 2B, right-hand panel). No internal anti-HA labeling was detected at time zero (Fig. 2B, left-hand panel), confirming the cells remain intact during the antibody labeling procedure. These results demonstrate HA-KCC2 undergoes constitutive endocytosis in HEK293 cells.

To confirm HA-KCC2 endocytosis is CME dependent, as suggested by our finding that neuronal KCC2 interacts with the clathrin adaptor AP-2 (Fig. 1 A), we analyzed the endocytosis of HA-KCC2 in HEK293 cells in the presence of two dominant-negative (DN) mutants of CME. These are (i) the GTPase Dynamin-2 mutant lysine (K) 44 to alanine (A), which lacks the GTP hydrolysis activity required for the scission of clathrin-coated

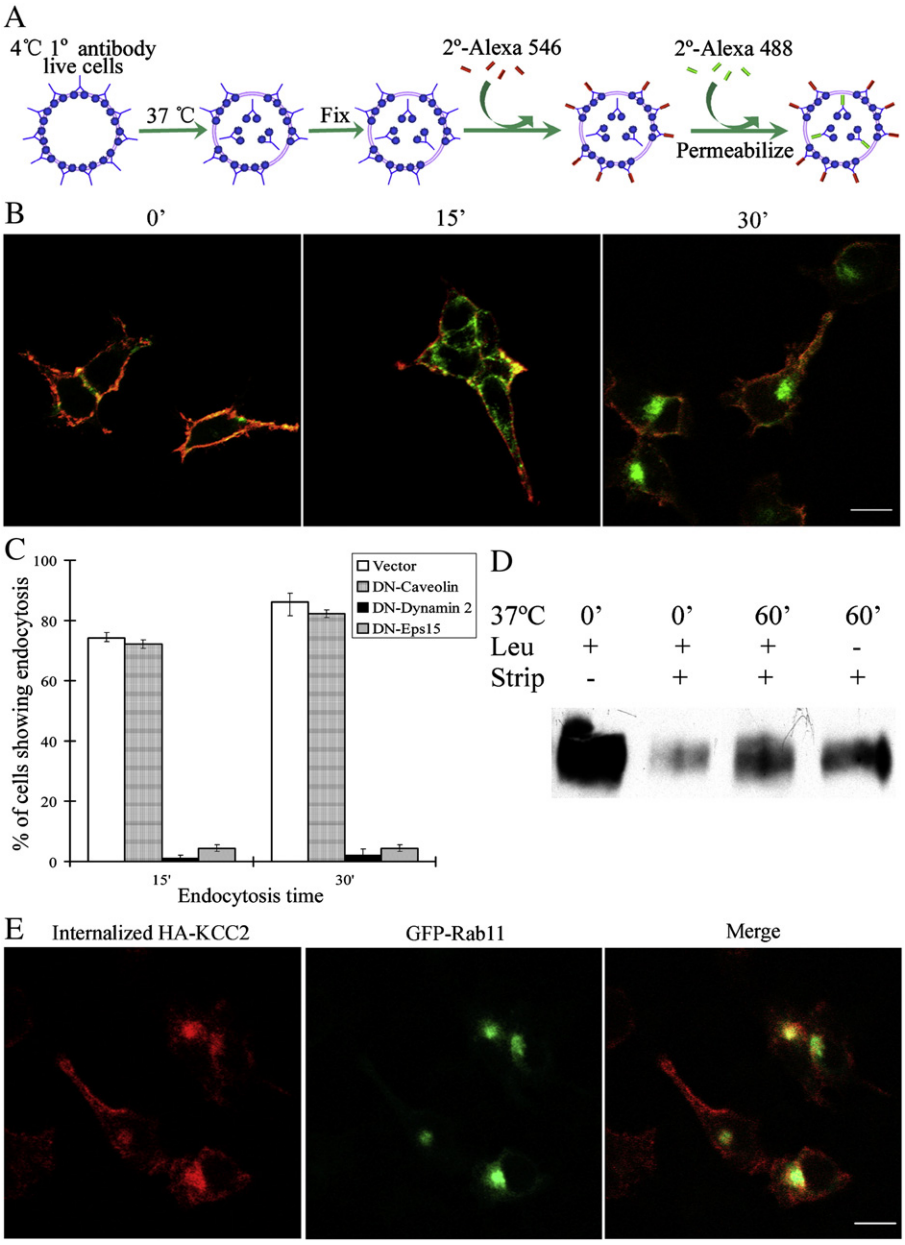

Fig. 2. KCC2 is internalized by clathrin-mediated endocytosis and targeted to the endosomal-recycling pathway. (A) Schema illustrating the fluorescence-based endocytosis assay, for details see Materials and methods. (B) Endocytosis of HA-KCC2. HEK293 cells transfected with HA-KCC2 were assayed for anti-HA internalization using a monoclonal antibody to HA, as depicted in (A). Shown are representative confocal images of surface anti-HA (red) and internalized anti-HA (green) at 0, 15 and 30 min. (C) Dominant-negative mutants of the clathrin-mediated endocytic pathway block HA-KCC2 endocytosis. HEK293 cells transiently expressing HA-KCC2 and either GFP vector (control, white bars), GFP-DN-Caveolin (checked bars), GFP-Dynamin-2 (K44A) (black bars), or GFP-Eps15(Δ95/295) (grey bars) were assayed as described in (B) and HA-KCC2 endocytosis at 15 and 30 min quantified as described in Materials and methods. Note, only permeabilized anti-HA labelling was performed with Alexa-546 secondary antibodies. Data are expressed as the percentage of cells that internalized anti-HA and presented as mean ± s.e ($n = 3$). (D) Internalized HA-KCC2 is not targeted for lysosomal degradation. Cell surface biotinylation was performed using the non-permeable cleavable biotinylation reagent Sulfo-NHS-SS-Biotin (1 mg/ml), on HA-KCC2 transfected cells incubated +/− leupeptin (Leu, 100 μg/ml) to inhibit lysosomal degradation and HA-KCC2 internalization assayed as described in Materials and methods. A typical immunoblot is shown detecting from left to right, total initial surface HA-KCC2 (0′, +Leu, −strip), strip control (0′, +Leu, +strip), HA-KCC2 internalized plus leupeptin (60′, +Leu, +strip) and HA-KCC2 internalized no leupeptin (60′, −Leu, +strip), using an anti-KCC2 antibody. (E) Internalized HA-KCC2 co-localizes with the recycling endosomal marker, Rab11. HEK293 cells transiently expressing HA-KCC2 and GFP tagged Rab11 were labelled with anti-HA for 30 min at 37 °C, then remaining surface bound anti-HA stripped as described in Materials and methods and internalized anti-HA detected with Alexa-546 secondary antibodies. Shown are representative images ($n = 3$) of internalized anti-HA (red) GFP-Rab11 (green) and the merge (yellow) illustrating co-localization of the proteins. Scale bar: 10 μm. (For interpretation of the references to colour in this figure legend, the reader is referred to the web version of this article.)

pits from the plasma membrane [32] and (ii) the epidermal growth factor receptor pathway substrate 15 mutant (Eps15Δ95/295) that lacks the second and third Eps15-Homology (EH) domains of Eps15, which inhibits AP-2 docking to the plasma membrane [33]. HEK293 cells were transfected with HA-KCC2 and either GFP, GFP-Dynamin-2 (K44A) or GFP-Eps15(Δ95/295). HA-KCC2 endocytosis was then analyzed by the antibody uptake assay, except in this experiment only permeabilized anti-HA labeling was detected with Alexa-546 labeling, after the removal of surface bound anti-HA. The proportion of GFP transfected cells showing internalized anti-HA labeling at 15 and 30 min of internalization was then quantified as described in Materials and methods. HA-KCC2 internalization in HA-KCC2 and GFP vector cotransfected cells was detected in 74.17 ± 1.2% and 86.11 ± 4.5% of transfected cells at 15 and 30 min respectively (Fig. 2C). While in contrast, cotransfection with either GFP-Dynamin-2 (K44A) or GFP-Eps15(Δ95/295) resulted in a reduction in HA-KCC2 internalization, with internalization detectable only in 1.1 ± 1.1% and 4.4 ± 1.1% of cells at 15 min and 2.2 ± 1.9% and 4.4 ± 1.1% of cells at 30 min respectively (Fig. 2C). As Dynamin-2 is also required for the alternate internalization pathway, the caveolin-dependent pathway [34], we examined whether the DN-Caveolin-GFP mutant [35] altered HA-KCC2 endocytosis. We found 72.22 ± 1.4% and 82.22 ± 1.4% of cells were internalized at 15 and 30 min respectively, which was comparable to HA-KCC2 alone transfected cells (Fig. 2C) and indicates GFP-DN-Caveolin does not affect HA-KCC2 endocytosis. Therefore together these results demonstrate that the constitutive endocytosis of HA-KCC2 is CME dependent.

The perinuclear localization of internalized HA-KCC2 (Fig. 2B) is reminiscent of the localization of internalized proteins, such as the transferrin receptor, to the endocytic recycling compartment [36]. Suggesting therefore that internalized HA-KCC2 may be trafficked via the endocytic-recycling pathway. To examine this, we first wanted to establish that internalized HA-KCC2 is not targeted for lysosomal degradation. To do this, we compared the stability of newly internalized HA-KCC2 in cells treated in the absence or presence of the lysosomal inhibitor, leupeptin. HEK293 cells transfected with HA-KCC2 were pre-treated with leupeptin (where indicated) and surface labeled with the cleavable form of biotin, Sulfo-NHS-SS-biotin, at 4 °C to arrest membrane trafficking. After biotin labeling, cells were incubated at 37 °C for 60 min (again with leupeptin where indicated) to allow endocytosis and intracellular trafficking to occur. Biotinylated proteins remaining at the cell surface were then cleaved (+strip, Fig. 2D) or not (−strip, Fig. 2D) with membrane impermeant reduced glutathione and remaining biotinylated proteins isolated by streptavidin column purification. Subsequently surface expressed (−strip, Fig. 2D) and internalized HA-KCC2 (+strip, Fig. 2D), +/−leupeptin treatment was detected and quantified by Western blotting (anti-HA). This analysis showed that the amount of internalized HA-KCC2 after 60 min is unaltered by leupeptin treatment (Fig. 2D), indicating endocytosed HA-KCC2 is not targeted for lysosomal degradation in HEK293 cells. Having established this, we next examined whether the compact perinuclear localization of internalized HA-KCC2 at 30 min (Fig. 2B) is representative of localization to the endosomal-recycling compartment. For this, we co-transfected HA-KCC2 with GFP tagged-rab11, an established marker for recycling endosomes [37]. We found internalized HA-KCC2 detected by the HA.11 uptake assay co-localizes with the GFP-rab11 labeled endocytic-recycling compartment after 30 min (Fig. 2E). Taken together these results demonstrate constitutively internalized KCC2 is trafficked via the endosomal-recycling pathway and not targeted for lysosomal degradation.

3.4. The KCC2 carboxy tail contains constitutive endocytosis signals

Sequence specific motifs directing the endocytosis of different classes of transporters are in many instances located within the intracellular amino (N) or carboxy (C) termini of these proteins [22–24]. Therefore we next examined whether either the intracellular N-

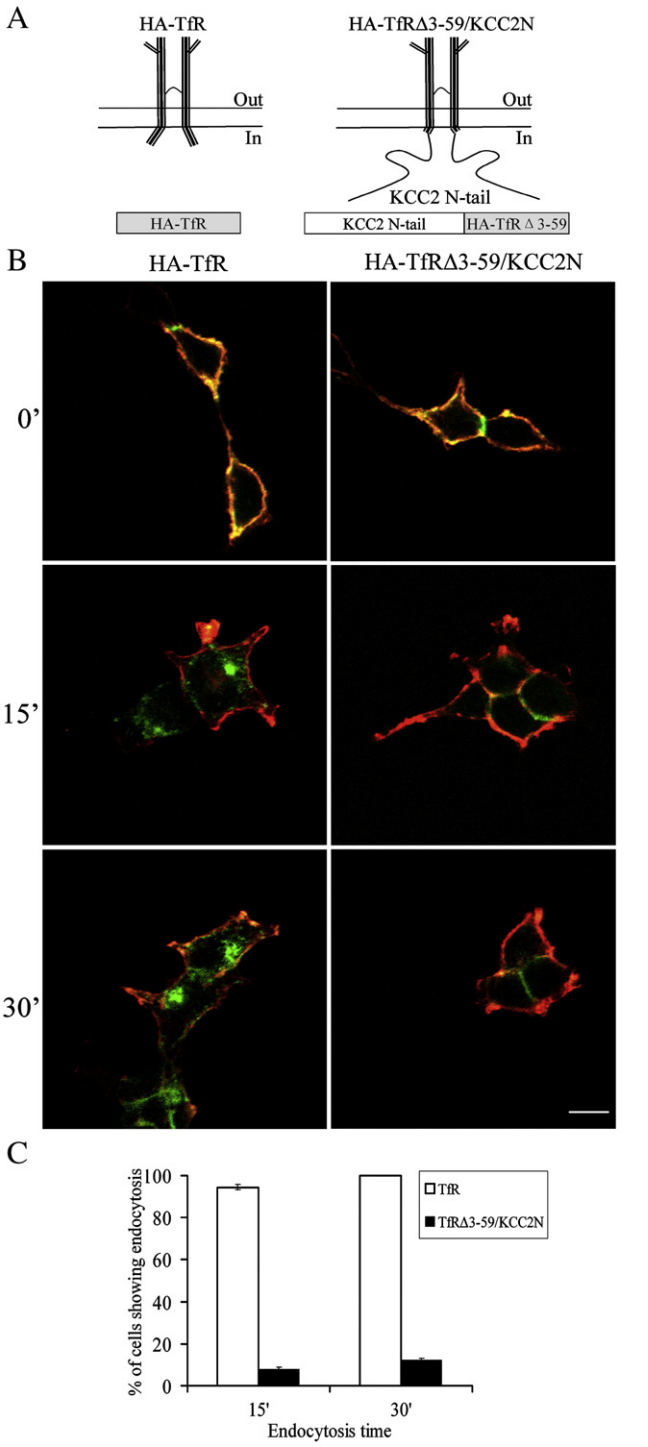

Fig. 3. The KCC2 amino (N) terminus does not mediate endocytosis. (A) Schematic illustration of HA-tagged Transferrin receptor (HA-TfR, left) and HA-TfR(Δ3–59) KCC2 N-tail chimera (HA-TfRΔ3-59/KCC2N, right). The N-tail (amino acids 3–95) of TfR was replaced with KCC2 N-tail (amino acids 2–102) to produce HA-TfRΔ3–59/KCC2N. (B) Endocytosis of HA-TfR and HA-TfRΔ3–59/KCC2N. HEK293 cells transfected with HA-TfR or HA-TfRΔ3–59/KCC2N were assayed for anti-HA internalization as depicted in Fig. 2A. Shown are representative confocal images of surface anti-HA (red) and internalized anti-HA (green) at 0, 15 and 30 min. Note internalized HA-TfR (green) was detected at 15 and 30 min, with no corresponding internalized HA-TfRΔ3–59/KCC2N at these time points, indicating the lack of endocytic signals in the KCC2 N-tail. Scale bar: 10 μm. (C) Quantification of HA-TfR (white bars) and HA-TfRΔ3–59/KCC2N (black bars) endocytosis at 15 and 30 min. Data are expressed as the percentage of cells that internalized anti-HA and presented as mean ± s.e (n = 3). (For interpretation of the references to colour in this figure legend, the reader is referred to the web version of this article.)

or C-terminus of KCC2 contains a functional endocytic signal(s). For this, we fused the KCC2 N and C termini respectively to the endocytosis deficient proteins, the intracellular domain deletion (Δ3–59) of the transferrin receptor (TfRΔ3–59, HA-tagged, Fig. 3A) and the interleukin 2 receptor α-chain (Tac, Fig. 4A) [23,38] and assessed their endocytic abilities. We chose these two approaches: to fuse KCC2 N- and C-terminus to the N-terminus of the TfR deletion (Δ3–59) and the C-terminus of the Tac protein respectively, in order to maintain the natural orientation of each of the KCC2 domains. Fusion of a viable autonomous endocytic motif is known to rescue the endocytosis deficiency of these two constructs [23,38,39]. First using the fluorescence-based endocytosis assay with anti-HA.11, we found wild-type HA-TfR efficiently endocytosed (Fig. 3B), with HA-TfR internalization detected in 94.4±1.1% and 100% cells after 15 and 30 min respectively (Fig. 3C). However in contrast HA-TfRΔ3-59/KCC2N, in which the TfR N-terminus (amino acids 3–59) is replaced with the KCC2 N-terminus (amino acids 2–102), was not able to internalize efficiently in our assay (Fig. 3B). HA-TfRΔ3-59/KCC2N internalization was detected in only 7.8±1.1% and 12.2±1.1% of cells after 15 and 30 min respectively (Fig. 3C). We confirmed this was not due to a defect in the total or cell surface expression of the HA-TfRΔ3-59/KCC2N protein (data not shown), suggesting therefore that the KCC2 N-tail does not contain an endocytic motif. Next we examined whether the KCC2 C-tail contains a functional endocytic motif, we assayed the internalization efficiency of Tac and Tac-C in which the KCC2 C-terminus (amino acids 635–1115) is fused in frame to the C-terminus of Tac (Fig. 4A). To follow their internalization we used the fluorescence-based endocytosis assay in combination with an anti-Tac antibody. From this analysis we found Tac, as previously reported [39], did not internalize from the plasma membrane after either 15 or 30 min of incubation at 37 °C (Fig. 4B,C). However in sharp contrast Tac-C, efficiently internalized at both 15 and 30 min (Fig. 4B). Internalization of Tac-C was detected in 96.7±1.9% and 100% of cells after 15 and 30 min respectively, compared to zero cells for Tac (Fig. 4C). Taken together these results demonstrate the KCC2 C-terminus, but not the N-terminus contains a constitutive endocytic motif(s).

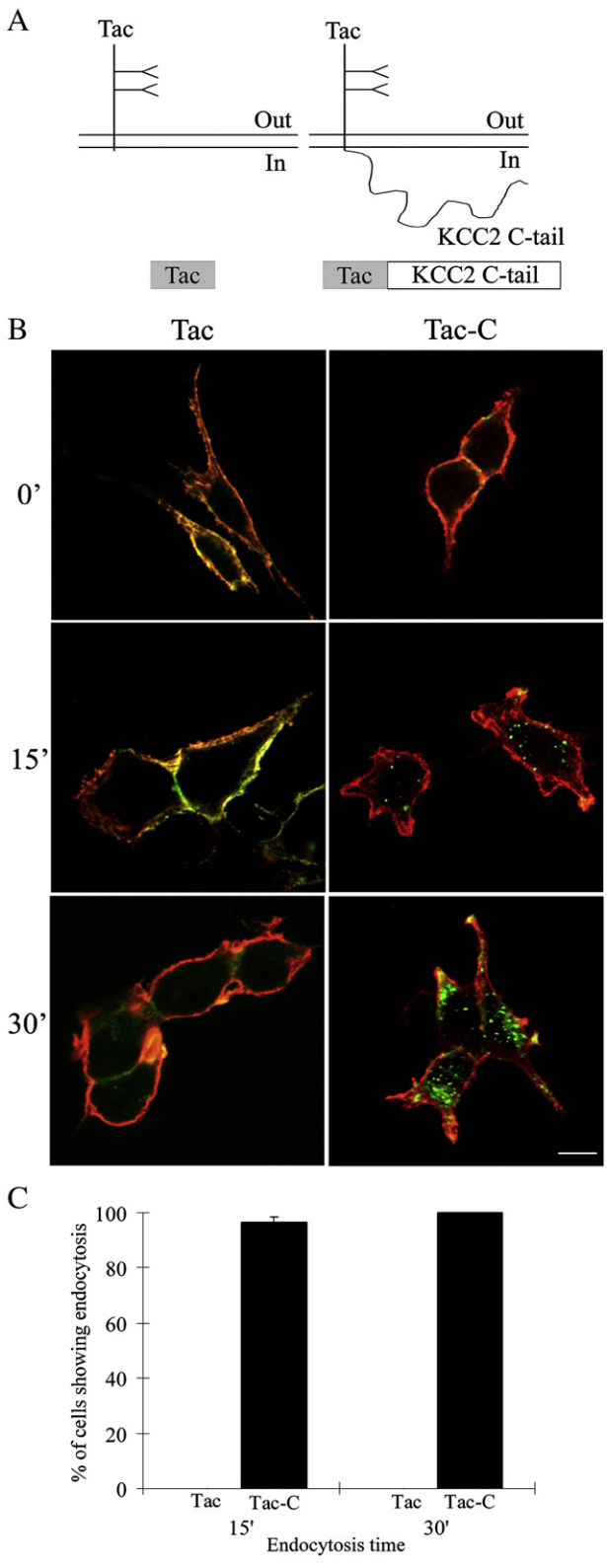

Fig. 4. KCC2 carboxy (C) terminus is sufficient to target Tac for endocytosis. (A) Schematic illustration of the interleukin receptor 2 alpha subunit intracellular truncation mutant (Tac, left) and the Tac/KCC2 C-tail chimera (Tac-C, right). The KCC2 C-tail (amino acids 635–1115) was fused to the C-terminus of Tac to produce Tac-C. (B) Endocytosis of Tac and Tac-C. HEK293 cells transfected with Tac or Tac-C were assayed for internalization using a monoclonal antibody to Tac as depicted in Fig. 2A. Shown are representative confocal images of surface anti-Tac (red) and internalized anti-Tac (green) at 0, 15 and 30 min. Note internalized Tac-C (green) was detected at 15 and 30 min, while Tac did not internalize at these time points, indicating the KCC2 C-tail contains an autonomous endocytic signal. Scale bar: 10 μm. (C) Quantification of Tac (white bars) and Tac-C (black bars) endocytosis at 15 and 30 min. Data are expressed as the percentage of cells that internalized anti-Tac and presented as mean±s.e (n=3). (For interpretation of the references to colour in this figure legend, the reader is referred to the web version of this article.)

3.5. KCC2 C-terminus amino acids 651–662 encompasses a discrete endocytic motif

In order to map the region of the C-tail containing the putative endocytic motif, we generated a series of progressive carboxyl truncations of Tac-C (Tac-CD1-6, Fig. 5A), and assessed each truncated protein for its ability to internalize. Prior to performing the endocytosis assays, each construct was confirmed for production of the correct length protein and to be expressed at the cell surface (data not shown). Using the fluorescence-based endocytosis assay with anti-Tac, we found the Tac constructs, Tac-CD1–Tac-CD5 (Fig. 5A), which correspond to the progressive carboxyl deletion of KCC2 residues 663–1115, all internalized as efficiently as Tac-C (see Fig. 5C), suggesting the endocytic motif(s) lies within the first 28 amino acids of the KCC2 C-tail. In contrast when we compared the internalization ability of Tac-CD5 to a Tac-CD6 construct, in which a further deletion of residues 651–662 was made (Fig. 5A), we found Tac-CD6 did not internalize (Fig. 5B). Tac-CD6 internalization was detected only in 3.3±4.1% cells compared to 100% cells for Tac-CD5

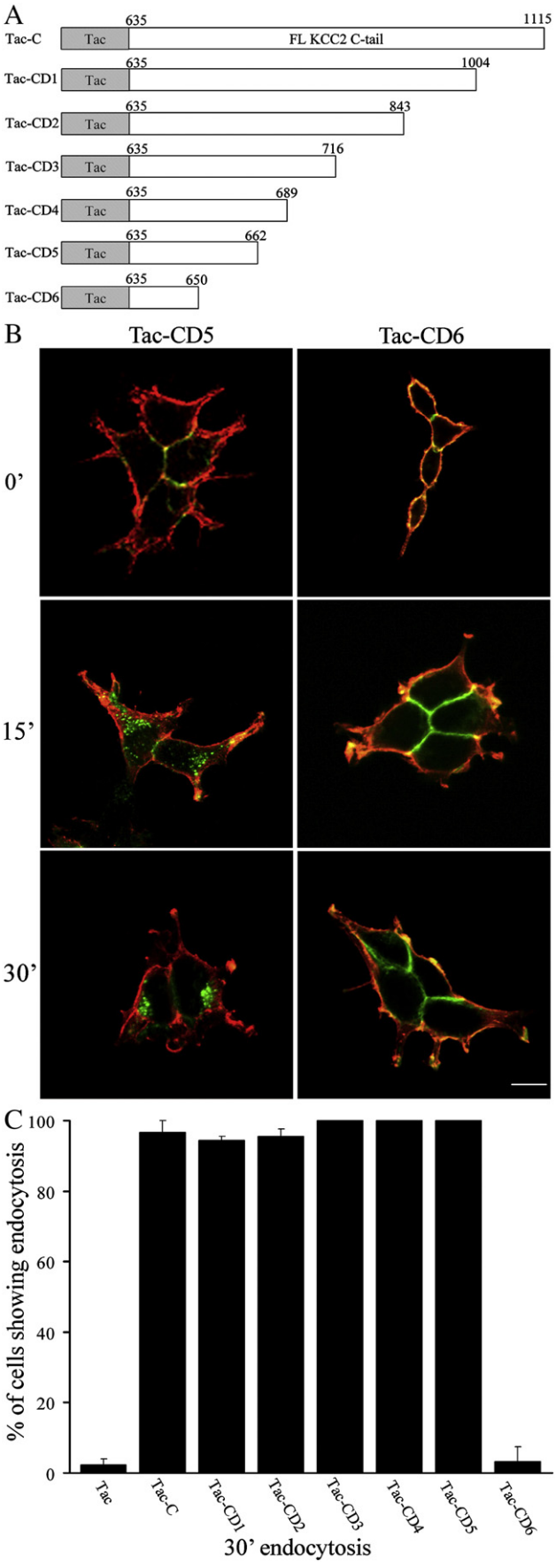

after 30 min (Fig. 5C). This data indicates the 12 amino acids present in the CD5 but absent in the CD6 fragment of KCC2 C-tail, which correspond to amino acids 651–662 of the mature KCC2 protein, contain an endocytic motif(s).

3.6. Identification of a novel di-leucine endocytic motif

Within these 12 amino acids unique to the CD5 construct (Fig. 6A) we observed that there is a classical tyrosine (Y)-based endocytic sequence $_{655}$YALL$_{658}$, which conforms to the consensus YXXφ (where X represents any amino acid and φ is a bulky hydrophobic amino acid). These YXXφ motifs have been shown to mediate clathrin dependent endocytosis through binding of the clathrin AP-2 complex [28]. In addition, within this sequence there is a di-leucine $_{657}$LL$_{658}$ that could also constitute an endocytic clathrin AP-2 complex binding motif [28]. Di-leucine motifs though are usually preceded by an acidic residue within the consensus, (D/E)XXXL(L/I), where D=aspartic acid, E=glutamic acid and I=isoleucine [28]. In KCC2, this acidic residue is replaced by an alanine $_{653}$**A**RYALL$_{658}$. However we noticed that there is a di-glutamic acid sequence located after the di-leucine $_{657}$LLRL**EE**$_{662}$. Hence, we postulated this di-leucine sequence might alternatively represent the potential endocytic motif. Therefore to test whether the tyrosine or the di-leucine motif mediate the endocytosis of Tac-CD5, we used alanine substitution mutagenesis to generate Tac-CD5(Y655A) and Tac-CD5(LL657,658AA) (Fig. 6A), knocking out each of the potential motifs independently. We then transfected these constructs into HEK293 cells and compared their endocytosis to wild type Tac-CD5, using the fluorescence-based endocytosis assay. We found Tac-CD5(Y655A) internalized similarly to wild-type Tac-CD5 (Fig. 6B), with internalization of Tac-CD5(Y655A) detected in 95.6±2.1% of cells after 30 min compared to 100% cells for wild type Tac-CD5 (Fig. 6C). In contrast, Tac-CD5(LL657,658AA) internalized very inefficiently (Fig. 6B), with internalization detected in only 2.5±2.8% (n=3, p<0.01) of cells after 30 min (Fig. 6C). Similar endocytosis rates for these Tac-CD5 mutants were also observed at the 15 min internalization time point (data not shown). These results indicate the di-leucine residues ($_{657}$LL$_{658}$) and not tyrosine-655 are important for the membrane internalization potential of Tac-CD5.

The importance and role of each of the leucine residues for the internalization of Tac-CD5 was next tested, by generating individual leucine to alanine substitute mutants (L657A and L658A, Fig. 6A) and internalization evaluated as described above. We found that the L657A substitution had a mild effect on Tac-CD5 endocytosis, with Tac-CD5 (L657A) internalization detected in 67.8±8.7% (n=3, p<0.05) cells after 30 min compared to 100% cells to wild type Tac-CD5 (Fig. 6C). In contrast the L658A substitution had a bigger effect on endocytosis, with Tac-CD5(L658A) internalization detected only in 13.3±1.9% (n=3, p<0.01) cells after 30 min (Fig. 6C). These results indicate both leucine residues are required to mediate efficient endocytosis of Tac-CD5, but that of the two; the second leucine (L658) is the most important residue.

The di-leucine $_{657}$LL$_{658}$ as mentioned above is not present within a classical acidic-di-leucine endocytic motif consensus, but acidic residues are found after the di-leucine sequence. As previous studies

Fig. 5. KCC2 C-terminus residues 651–662 contain an endocytic motif. (A) Schematic illustration of the Tac-C carboxyl truncation constructs, Tac-CD1-CD6. The KCC2 C-tail amino acids contained in each construct are shown. (B) Endocytosis of Tac-CD5 and Tac-CD6. HEK293 cells transfected with Tac-CD5 (left) or Tac-CD6 (right) were assayed for anti-Tac internalization as depicted in Fig. 2A. Shown are representative confocal images of surface anti-Tac (red) and internalized anti-Tac (green) at 0, 15 and 30 min. Note internalized Tac-CD5 (green) was detected at 15 and 30 min, while no internalized Tac-CD6 was detected at any time point. Scale bar: 10 μm. (C) Quantification of Tac-C carboxyl truncation constructs endocytosis at 30 min. Data are expressed as the percentage of cells that internalized anti-Tac and presented as mean±s.e (n=3). Data from (B) and (C) indicate the endocytic motif is located within amino acids 651–662 of the mature KCC2 protein. (For interpretation of the references to colour in this figure legend, the reader is referred to the web version of this article.)

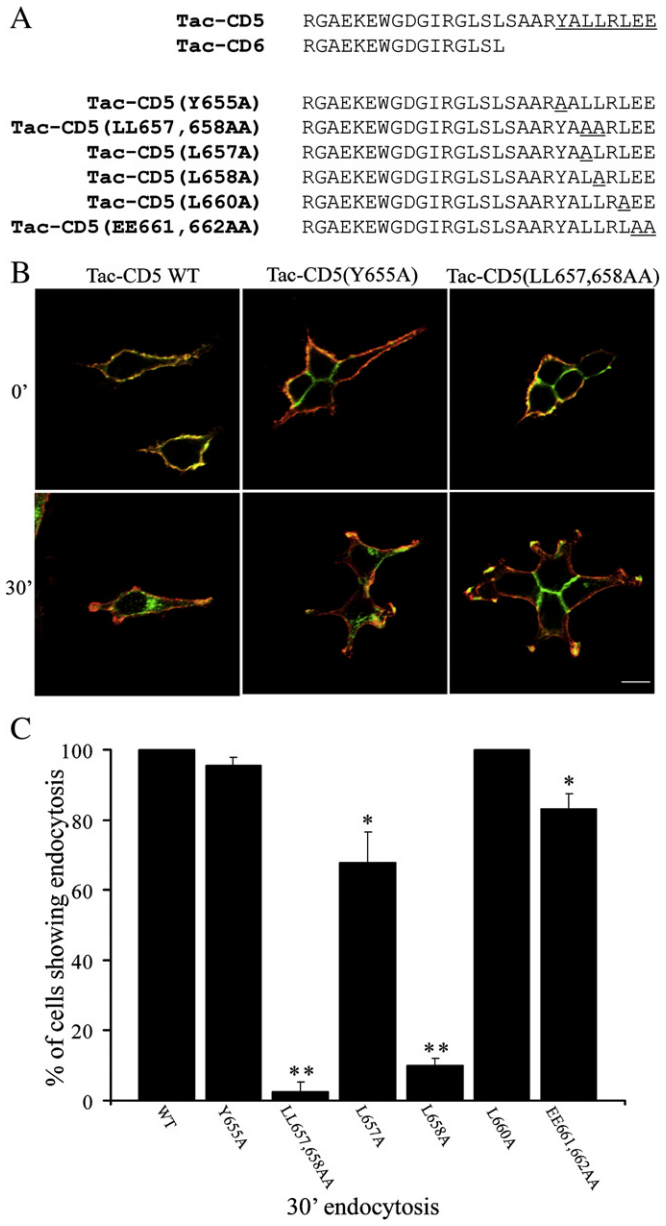

Fig. 6. Identification of a di-leucine based endocytic motif within KCC2 C-terminus amino acids 651–662. (A) *Top*, Alignment of the KCC2 amino acid sequence in the CD5 (635–662) and CD6 (635–650) regions of KCC2. Note the amino acids containing the potential YXXφ and LL endocytic motifs are underlined. *Bottom*, alignment of the different Tac-CD5 point mutation mutants. The alanine-substituted amino acid residues are underlined. (B) Endocytosis of Tac-CD5, Tac-CD5(Y655A), and Tac-CD5(LL657, 658AA). HEK293 cells transfected with Tac- CD5(WT) wild-type (left), Tac-CD5(Y655A) (middle), or Tac-CD5(LL657, 658AA) (right) were assayed for anti-Tac internalization as depicted in Fig. 2A. Shown are representative confocal images of surface anti-Tac (red) and internalized anti-Tac (green) at 0 and 30 min. Note no internalization of Tac-CD5 (LL657, 658AA) was detected at 30 min, while Tac-CD5 and Tac-CD5(Y655A) both internalized. Scale bar: 10 μm. (C) Quantification of Tac-CD5 wild type and the CD5 mutant endocytosis at 30 min. Data are expressed as the percentage of cells that internalized anti-Tac and presented as mean±s.e (n=3). Significant differences from control (wild type Tac-CD5) were found (*p<0.05, **p<0.01) using the Student's t-test, two tails. (For interpretation of the references to colour in this figure legend, the reader is referred to the web version of this article.)

have indicated the importance of the amino acid residues surrounding the di-leucine for the potency of the endocytic signal [28], we decided to examine the role of the residues surrounding the $_{657}$LL$_{658}$ motif. Specifically we tested the role of L660 and the two glutamic acid residues $_{661}$EE$_{662}$ following the di-leucine residues. Again we generated alanine substitution mutants in the context of the Tac-CD5 construct. Tac-CD5(L660A) and Tac-CD5(EE661,662AA) (Fig. 6A) were tested for their ability to internalize in our endocytosis assay. We found Tac-CD5(L660A) internalized as efficiently as wild type Tac-CD5 (Fig. 6C), with internalization detected in 100% cells after 30 min. In contrast we found Tac-CD5(EE661,662AA) internalization was affected, with internalization of Tac-CD5(EE661,662AA) detected only in 83.3±4.2% (n=3, p<0.05) after 30 min (Fig. 6C). This result suggests acidic residues $_{661}$EE$_{662}$ form part of the endocytic motif, but perhaps play a minor role in Tac-CD5 internalization compared to the di-leucine residues, $_{657}$LL$_{658}$. Taken altogether the results of the alanine mutagenesis experiments demonstrate there is an endocytosis motif in the region encompassing amino acids 657–662 of KCC2, which is a novel acidic di-leucine endocytic motif, $_{657}$LLXXEE$_{662}$.

3.7. The di-leucine residues $_{657}$LL$_{658}$ comprise the only endocytosis motif in the KCC2 C-terminus

Our findings so far strongly suggest the identified di-leucine motif is the only endocytic motif within the full-length KCC2 C-terminus. To test and confirm this, we generated the Tac-C(LL657,658AA) mutant by site-directed mutagenesis and assessed its ability to endocytose using the fluorescence-based endocytosis assay, with the anti-Tac antibody. As controls for this assay, we used Tac-C and also generated a Tac-C(Y665A) mutant, which according to our results with Tac-CD5 (Y665A) (Fig. 6), should internalize as efficiently as Tac-C. We found, as predicted that Tac-C(Y665A) internalized similarly to wild type Tac-C (Fig. 7A), with internalization of Tac-C(Y665A) and wild type Tac-C detected in 90±3.3% cells and 95.6±2.2% after 15 min and 95.6±2.2% and 100% of cells after 30 min, respectively (Fig. 7B). In contrast, Tac-C (LL657,658AA) endocytosed poorly (Fig. 7A), with Tac-C(LL657,658AA) internalization detectable only in 3.3±1.9% and 6.7±3.8% of cells after 15 and 30 min respectively. These results demonstrate the di-leucine motif is the only functional endocytosis motif within the context of the full length KCC2 C-tail and is both necessary and sufficient for the endocytosis-targeting function of the KCC2 C-tail.

3.8. The di-leucine motif is essential for KCC2 constitutive endocytosis

Finally, we examined whether the di-leucine motif is required for the constitutive endocytosis of full length KCC2. For this, the HA-KCC2 (LL657,658AA) mutant was generated by site-directed mutagenesis and the endocytosis of this mutant and wild type HA-KCC2 in transiently transfected HEK293 cells were quantified using the surface biotinylation endocytosis assay. The advantage of using this quantitative assay versus the fluorescent approach was that we could determine whether internalization is blocked or if only the rate of endocytosis is altered. The endocytosis assay was performed essentially as described (Fig. 2D) on HEK293 cells transfected with either HA-KCC2 or HA-KCC2(LL657,658AA). Following the endocytosis assay, biotinylated HA-KCC2 variants both surface expressed (−strip, Fig. 8A) and internalized (+strip, Fig. 8A) were detected by streptavidin purification followed by Western blot detection with a KCC2 antibody. Western blots were subsequently quantified by densitometry. We found both wild type HA-KCC2 and HA-KCC2(LL657,658AA) expressed efficiently at the cell surface (0′, −strip, Fig. 8A) and that glutathione stripping at 0 min removed the majority of remaining surface biotinylated HA-KCC2 and HA-KCC2(LL657,658AA) (0′, +strip, Fig. 8A). Residual glutathione-resistant biotinylated protein was then considered as background and subtracted from the signal derived from further incubation time points. After 30 min incubation at 37 °C (endocytosis), we detected an increased amount of biotinylated HA-KCC2 protected from glutathione stripping (30′, +strip, left panel Fig. 8A), which represents the amount of internalized HA-KCC2 and equates to 5±1.1% of surface expressed wild type HA-KCC2 (Fig. 8B). In contrast, we observed no increase in the amount of biotinylated HA-

KCC2(LL657,658AA) protected from glutathione stripping after 30 min (30′, +strip, right panel Fig. 8A), indicating HA-KCC2(LL657,658AA) did not internalize (Fig. 8B). Hence we demonstrate that the LL657,658AA mutation is sufficient to block HA-KCC2 internalization, thus indicating that $_{657}$LL$_{658}$, is essential for the constitutive endocytosis of HA-KCC2.

In Fig. 1 we have shown that endogenous neuronal KCC2 is associated with the CME machinery through binding to the CME pathway AP-2 complex. Suggesting therefore that KCC2 endocytosis may be mediated via the binding of this adaptor complex. We therefore tested whether $_{657}$LL$_{658}$, which is essential for the constitutive endocytosis of KCC2 is the binding domain for the AP-2 complex. To examine this, we tested the binding abilities of HA-KCC2 and HA-KCC2(LL657,658AA) to the α-adaptin subunit of AP-2 by co-immunoprecipitation. Immunoprecipitated complexes were prepared from whole cell lysates of HEK293 cells transiently transfected with HA-KCC2 or HA-KCC2(LL657,658AA), using a mouse monoclonal antibody to HA or pre-immune mouse IgG as the control. These immunoprecipitates were then Western blotted with antibodies to HA and α-adaptin. We found α-adaptin was present in the anti-HA immunoprecipitates isolated from HA-KCC2 expressing cells but not HA-KCC2(LL657,658AA) expressing cells or in the control immunoprecipitates (Fig. 8C). This confirms that transiently expressed HA-KCC2 interacts with the AP-2 complex of HEK293 cells and that the LL657,658AA mutation is sufficient to block the binding of α-adaptin and the AP-2 complex to KCC2. Taken together with the Tac-CD5 (Fig. 6) and Tac-C (Fig. 7) data, these results demonstrate that we have identified a di-leucine based endocytosis motif that is essential for the

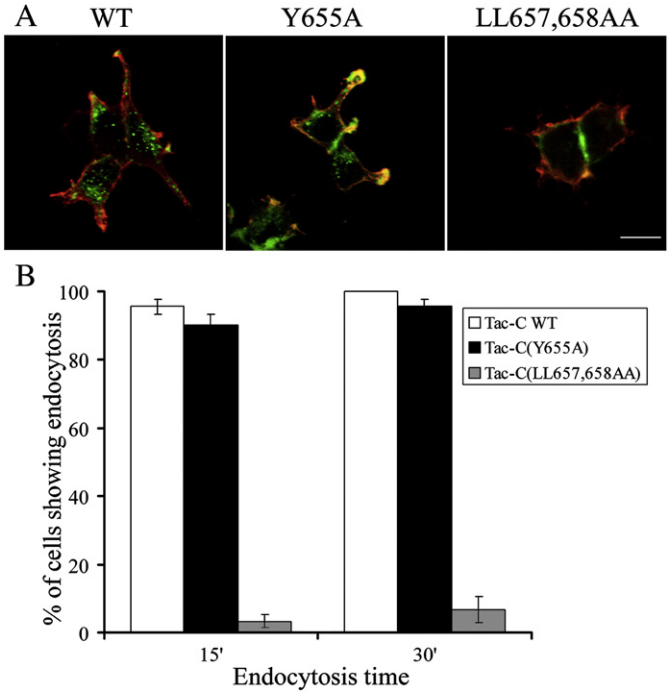

Fig. 7. Di-leucine residues $_{657}$LL$_{658}$ are necessary for Tac-C endocytosis. (A) Endocytosis of Tac-C, Tac-C(Y655A), and Tac-C(LL657, 658AA). HEK293 cells transfected with Tac-C (WT, left), Tac-C(Y655A) (middle), or Tac-C(LL657, 658AA) (right) were assayed for anti-Tac internalization as depicted in Fig. 2A. Shown are representative confocal images of surface anti-Tac (red) and internalized anti-Tac (green) at 30 min. Note no internalization of Tac-C(LL657, 658AA) was detected, while Tac-C and Tac-C (Y655A) both internalized. Scale bar: 10 μm. (B) Quantification of Tac-C wild type (white bars), Tac-C (Y655A) (black bars) and Tac-C(LL657, 658AA) (grey bars) endocytosis at 15 and 30 min. Data are expressed as the percentage of cells that internalized anti-Tac (n=3) and presented as mean±s.e. (For interpretation of the references to colour in this figure legend, the reader is referred to the web version of this article.)

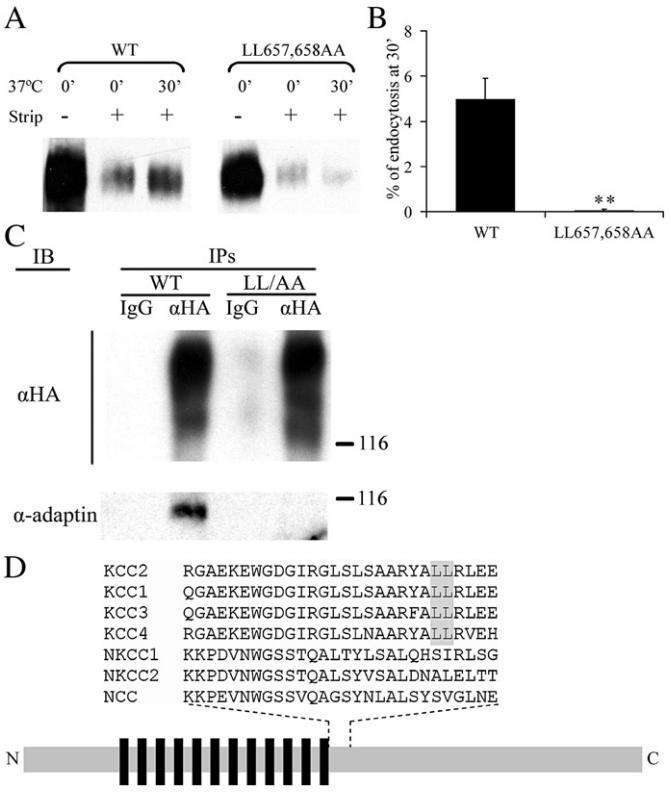

Fig. 8. Di-leucine $_{657}$LL$_{658}$ is essential for the constitutive endocytosis of HA-KCC2. (A) Comparison of the endocytosis rates of HA-KCC2 and HA-KCC2(LL657, 658AA). Cell surface biotinylation was performed using the non-permeable cleavable biotinylation reagent Sulfo-NHS-SS-Biotin (1 mg/ml) on HA-KCC2 and HA-KCC2(LL657, 658AA) transfected cells and internalization detected as described in Materials and methods. Typical immunoblots are shown detecting from left to right, total initial surface (0′, −strip), strip control (0′, +strip) and internalization for 30 min (30′, +strip) for HA-KCC2 (*left*) and HA-KCC2 (LL657,658AA) (*right*), using an anti-KCC2 antibody. (B) Quantification of HA-KCC2 and HA-KCC2 (LL657, 658AA) endocytosis at 30 min. Data are expressed as the percentage of each internalized KCC2 variant at 30 min and presented as mean±s.e. (n=3). The difference in internalization between HA-KCC2 and HA-KCC2 (LL657,658AA) was found to be statistically significant (**$p<0.01$), using the Student's t-test, two tails. (C) Comparison of binding of the AP-2 complex α-adaptin subunit to HA-KCC2 and HA-KCC2(LL657, 658AA). Whole cell lysates from HA-KCC2 and HA-KCC2 (LL657, 658AA) transiently expressing HEK293 cells were immunoprecipitated (IP) with antibodies to HA or pre-immune mouse IgG, and Western blotted (IB) with antibodies to HA or α-adaptin. α-adaptin was co-immunoprecipitated with HA-KCC2 but not with HA-KCC2(LL657,658AA). (D) Amino acid sequence alignment of the first 28 residues of the mouse KCC2 carboxyl terminus with the orthologous region in other mouse cation-chloride cotransporters. The location of this region is marked by dashes on a schematic representation of the structure of a cation-chloride cotransporter. Black bars illustrate transmembrane domains. Note, the novel di-leucine endocytic motif identified in KCC2 is conserved in KCC1, KCC3 and KCC4 (shown shaded), but it is not found in NKCC1, NKCC2 or NCC.

CME dependent constitutive endocytosis of KCC2 via binding of the AP-2 complex.

4. Discussion

KCC2 is essential in the vast majority of CNS neurons for the development and maintenance of inhibitory neurotransmission [3–7]. In addition loss of KCC2 expression and function is associated with several neuropathological conditions including chronic pain [5], nerve injury [6] and epilepsy [7]. Given this seemingly crucial role for KCC2 in the mature nervous system, it was surprising how little was known of the cellular mechanisms controlling KCC2 stability and function, in particular how KCC2 surface expression is controlled. In this study we examined the cellular mechanisms controlling the endocytosis of KCC2. We show that (i) constitutive endocytosis of KCC2 is controlled by the clathrin mediated endocytic pathway, (ii) endogenous neuronal

KCC2 associates with the clathrin binding adaptor protein-2 complex, (iii) constitutively internalized KCC2 is sorted to the endosomal recycling pathway, (iv) KCC2 carboxy tail contains an autonomous endocytic signal and (v) this endocytic signal is a novel acidic di-leucine motif $_{657}$LLXXEE$_{662}$, which we show is both necessary and sufficient to mediate the binding of KCC2 to the AP-2 complex and the constitutive endocytosis of KCC2. Together our results reveal that the CME pathway and a discrete endocytic motif in the KCC2 carboxyl tail mediate the constitutive endocytosis of KCC2.

Our molecular mapping study is the first to report an endocytic motif in any CCC family protein. By generating a functional HA-tagged version of KCC2 (HA-KCC2, Fig. 1B–D), we were able to demonstrate that KCC2 constitutive endocytosis is CME pathway dependent (Fig. 2C). Whether other CCC family proteins are endocytosed also in a clathrin-dependent manner is yet to be determined. CME dependent endocytosis is largely controlled through the binding of clathrin adaptor complexes and our results indicate KCC2 binds *in vivo* to the clathrin binding AP-2 complex (Fig. 1A). In this study we initially identified a key 12 amino acid region $_{651}$SAARYALLRLEE$_{662}$ within the KCC2 carboxyl tail proximal to the last transmembrane domain (Fig. 5), encoding an autonomous endocytic signal. Using alanine substitution mutagenesis we then demonstrated that the di-leucine residues ($_{657}$LL$_{658}$) within this region are central to this endocytosis motif (Figs. 6,7). Finally we demonstrated that these residues are essential for the constitutive endocytosis of HA-KCC2 (Fig. 8A–B) and the binding of KCC2 to the AP-2 complex (Fig. 8C). Interestingly, we found that L658 plays a major role within the endocytosis motif whereas L657 plays a more minor role in conveying the endocytosis-targeting function of this di-leucine motif (Fig. 6). In addition we have shown that although these di-leucine residues are not present within a classical acidic di-leucine endocytic motif, (E/D)XXXL(L/I) [28], two glutamic acid residues downstream $_{657}$LLRLEE$_{662}$ are required for the full function of this endocytic motif (Fig. 6). This confirms previous findings that the composition of the surrounding amino acids can impact the function of an endocytosis motif [28]. An additional interesting finding from this mapping study was that although KCC2 has a potentially good tyrosine based endocytosis motif ($_{655}$YALL$_{658}$) within this region, it is apparently not utilized (Fig. 6). This was surprising and it will be of future interest to determine why this tyrosine motif is not used in KCC2 endocytosis, or if it plays an alternative targeting role for KCC2.

Sequence alignment of the region of the mouse KCC2 carboxyl tail containing the endocytic motif, with the same region of homologous murine cation-chloride co-transporters (Fig. 8D), reveals this novel KCC2 endocytic motif is highly conserved between related KCC family members. This suggests the mechanisms controlling the constitutive endocytosis of KCC family members may be conserved. Moreover this endocytic motif is not found in the analogous region of the more distally related NKCC1, NKCC2 or NCC proteins (Fig. 8D). Given the opposing physiological functions of KCC proteins versus NKCC and NCC proteins, in mediating either chloride efflux or influx respectively, the presence or absence of this endocytic motif provides further indication of how these related protein families may be differentially regulated. A role for specific regions of the KCC2 carboxyl terminus in controlling transporter activity has been reported [40,41], but how these regions mediate this function is as yet unknown. It is postulated that either acquired conformations or specific protein–protein interactions are involved. In this regard, it is interesting that we have mapped the KCC2 constitutive endocytosis motif to the C-tail of KCC2. Recent reports also indicate that KCC2 and other CCC family members encode the capacity to both homo and hetero-oligomerize [17–19,42]. The regions within these proteins mediating this function are beginning to be elucidated and an important role for the carboxyl tail yet again is indicated [42]. How both homo- and hetero-oligomerization impact on the function of our defined endocytic motif, will need to be addressed. For example does dimerization affect the availability of the endocytic motif? The mapping of the precise regions of the carboxyl tail required to form dimers will provide a starting point to address this question.

The endocytic motif identified in this study regulates the constitutive endocytosis of KCC2 (Fig. 2). Both seizure activity (BDNF dependent signaling) and oxidative stress (hydrogen peroxide induced) have been shown to induce a rapid reduction in KCC2 surface expression by enhancing KCC2 internalization in hippocampal neurons [14,15]. This suggests the additional existence of regulatory mechanisms that can enhance KCC2 constitutive endocytosis. This BDNF and oxidative stress dependent regulation of KCC2 surface expression [14,15] is associated with a reduction in tyrosine phosphorylation of KCC2 [15], suggesting that tyrosine phosphorylation or de-phosphorylation may be a means by which KCC2 endocytosis could be regulated. It will therefore be of interest to examine whether stress dependent regulation of KCC2 endocytosis utilizes the same endocytic motif we have mapped in this study. Also whether the tyrosine phosphorylation state of KCC2 controls the function of this endocytic motif, perhaps by altering its availability and its interaction with the endocytic machinery. A recent report has also indicated the additional existence of a protein kinase-C dependent inhibition of KCC2 endocytosis, involving the phosphorylation of a site in the KCC2 C-terminus distal to the novel endocytic motif reported here [43]. It will be interesting to examine whether this phosphorylation event also impacts the function of the novel KCC2 endocytosis motif reported in this study. Finally, we have shown that constitutively endocytosed KCC2 is targeted to the recycling endosomal pathway (Fig. 2). It will therefore also be of future interest to determine whether BDNF-signaling and oxidative stress also target KCC2 internalization to the recycling-endosomal pathway or alternatively for degradation.

Given the essential role of KCC2 in regulating the strength of inhibitory neurotransmission, membrane trafficking of KCC2 represents an optimal mechanism by which inhibition may be indirectly regulated. Our results defining the motif and mechanism by which the constitutive endocytosis of KCC2 is controlled, are an initial step in understanding the molecular determinants by which KCC2 transporter membrane trafficking may be regulated. Finally given the conservation of this motif amongst K^+/Cl^- family proteins, our studies are also applicable to examining how endocytosis is controlled in related KCC proteins and its impact on their function of controlling cellular chloride homeostasis in the many different tissues of the body in which these transporters are expressed.

Acknowledgements

We thank Julie Donaldson, Yves Rouille, Robert lodge, Mark McNiven, Matthew Mulvey, Robert Harvey, Peter McPherson and Stephane Laporte for constructs and antibodies. This work was supported, in part by the Canadian Institute of Health Research (CIHR) operating grant awarded to, F. B. (MOP-62822) and J.P. (MOP-49590). F.B. and D.B. are CIHR-Canada Research Chairs-Tier II recipients.

Appendix A. Supplementary data

Supplementary data associated with this article can be found, in the online version, at doi:10.1016/j.cellsig.2008.06.011.

References

[1] H. Betz, Q. Rev. Biophys. 25 (4) (1992) 381–394.
[2] W. Sieghart, Adv. Pharmacol. 54 (2006) 231–263.
[3] C. Rivera, J. Voipio, J.A. Payne, E. Ruusuvuori, H. Lahtinen, K. Lamsa, U. Pirvola, M. Saarma, K. Kaila, Nature 397 (6716) (1999) 251–255.
[4] C.A. Hubner, V. Stein, I. Hermans-Borgmeyer, T. Meyer, K. Ballanyi, T.J. Jentsch, Neuron 30 (2) (2001) 515–524.

[5] J.A. Coull, D. Boudreau, K. Bachand, S.A. Prescott, F. Nault, A. Sik, P. De Koninck, Y. De Koninck, Nature 424 (6951) (2003) 938–942.
[6] J. Nabekura, T. Ueno, A. Okabe, A. Furuta, T. Iwaki, C. Shimizu-Okabe, A. Fukuda, N. Akaike, J. Neurosci. 22 (11) (2002) 4412–4417.
[7] N.S. Woo, J. Lu, R. England, R. McClellan, S. Dufour, D.B. Mount, A.Y. Deutch, D.M. Lovinger, E. Delpire, Hippocampus 12 (2) (2002) 258–268.
[8] G. Huberfeld, L. Wittner, S. Clemenceau, M. Baulac, K. Kaila, R. Miles, C. Rivera, J. Neurosci. 27 (37) (2007) 9866–9873.
[9] K. Inoue, J. Yamada, S. Ueno, A. Fukuda, J. Neurochem. 96 (2) (2006) 598–608.
[10] K.T. Kahle, J. Rinehart, P. de Los Heros, A. Louvi, P. Meade, N. Vazquez, S.C. Hebert, G. Gamba, I. Gimenez, R.P. Lifton, Proc. Natl. Acad. Sci. U. S. A. 102 (46) (2005) 16783–16788.
[11] W. Kelsch, S. Hormuzdi, E. Straube, A. Lewen, H. Monyer, U. Misgeld, J. Neurosci. 21 (21) (2001) 8339–8347.
[12] S. Khirug, K. Huttu, A. Ludwig, S. Smirnov, J. Voipio, C. Rivera, K. Kaila, L. Khiroug, Eur. J. Neurosci. 21 (4) (2005) 899–904.
[13] H. Fiumelli, L. Cancedda, M.M. Poo, Neuron 48 (5) (2005) 773–786.
[14] C. Rivera, J. Voipio, J. Thomas-Crusells, H. Li, Z. Emri, S. Sipila, J.A. Payne, L. Minichiello, M. Saarma, K. Kaila, J. Neurosci. 24 (19) (2004) 4683–4691.
[15] H. Wake, M. Watanabe, A.J. Moorhouse, T. Kanematsu, S. Horibe, N. Matsukawa, K. Asai, K. Ojika, M. Hirata, J. Nabekura, J. Neurosci. 27 (7) (2007) 1642–1650.
[16] J.A. Payne, C. Rivera, J. Voipio, K. Kaila, Trends Neurosci. 26 (4) (2003) 199–206.
[17] M.L. Moore-Hoon, R.J. Turner, Biochemistry 39 (13) (2000) 3718–3724.
[18] J.C. de Jong, P.H. Willems, F.J. Mooren, L.P. van den Heuvel, N.V. Knoers, R.J. Bindels, J. Biol. Chem. 278 (27) (2003) 24302–24307.
[19] P. Blaesse, I. Guillemin, J. Schindler, M. Schweizer, E. Delpire, L. Khiroug, E. Friauf, H.G. Nothwang, J. Neurosci. 26 (41) (2006) 10407–10419.
[20] H.E. Melikian, K.M. Buckley, J. Neurosci. 19 (18) (1999) 7699–7710.
[21] P.A. Ortiz, Am. J. Physiol. Renal. Physiol. 290 (3) (2006) F608–616.
[22] H. Al-Hasani, R.K. Kunamneni, K. Dawson, C.S. Hinck, D. Muller-Wieland, S.W. Cushman, J. Cell. Sci. 115 (Pt 1) (2002) 131–140.
[23] K.L. Holton, M.K. Loder, H.E. Melikian, Nat. Neurosci. 8 (7) (2005) 881–888.
[24] U. Schmidt, S. Briese, K. Leicht, A. Schurmann, H.G. Joost, H. Al-Hasani, J. Cell. Sci. 119 (Pt 11) (2006) 2321–2331.
[25] S. D'Souza, A. Garcia-Cabado, F. Yu, K. Teter, G. Lukacs, K. Skorecki, H.P. Moore, J. Orlowski, S. Grinstein, J. Biol. Chem. 273 (4) (1998) 2035–2043.
[26] A.Y. Wong, A.M. Fay, D. Bowie, J. Neurosci. 26 (21) (2006) 5750–5755.
[27] R. Heir, C. Ablasou, E. Dumontier, M. Elliott, C. Fagotto-Kaufmann, F.K. Bedford, EMBO Rep. 7 (12) (2006) 1252–1258.
[28] J.S. Bonifacino, L.M. Traub, Annu. Rev. Biochem. 72 (2003) 395–447.
[29] T. Grampp, K. Sauter, B. Markovic, D. Benke, J. Biol. Chem. 282 (33) (2007) 24157–24165.
[30] J.T. Kittler, P. Delmas, J.N. Jovanovic, D.A. Brown, T.G. Smart, S.J. Moss, J. Neurosci. 20 (21) (2000) 7972–7977.
[31] A. Kyrozis, D.B. Reichling, J. Neurosci. Methods 57 (1) (1995) 27–35.
[32] H. Damke, T. Baba, D.E. Warnock, S.L. Schmid, J. Cell. Biol. 127 (4) (1994) 915–934.
[33] A. Benmerah, M. Bayrou, N. Cerf-Bensussan, A. Dautry-Varsat, J. Cell. Sci. 112 (Pt 9) (1999) 1303–1311.
[34] Q. Yao, J. Chen, H. Cao, J.D. Orth, J.M. McCaffery, R.V. Stan, M.A. McNiven, J. Mol. Biol. 348 (2) (2005) 491–501.
[35] L. Pelkmans, J. Kartenbeck, A. Helenius, Nat. Cell. Biol. 3 (5) (2001) 473–483.
[36] J.L. Martys, T. Shevell, T.E. McGraw, J. Biol. Chem. 270 (43) (1995) 25976–25984.
[37] O. Ullrich, S. Reinsch, S. Urbe, M. Zerial, R.G. Parton, J. Cell. Biol. 135 (4) (1996) 913–924.
[38] S. Belouzard, Y. Rouille, Embo J. 25 (5) (2006) 932–942.
[39] P.K. Tan, C. Waites, Y. Liu, D.E. Krantz, R.H. Edwards, J. Biol. Chem. 273 (28) (1998) 17351–17360.
[40] M.J. Bergeron, E. Gagnon, L. Caron, P. Isenring, J. Biol. Chem. 281 (23) (2006) 15959–15969.
[41] A. Mercado, V. Broumand, K. Zandi-Nejad, A.H. Enck, D.B. Mount, J Biol Chem 281 (2) (2006) 1016–1026.
[42] C.F. Simard, M.J. Bergeron, R. Frenette-Cotton, G.A. Carpentier, M.E. Pelchat, L. Caron, P. Isenring, J. Biol. Chem. 282 (25) (2007) 18083–18093.
[43] H.H. Lee, J.A. Walker, J.R. Williams, R.R. Goodier, J.A. Payne, S.J. Moss, J. Biol. Chem. (2007).